Geosci. Model Dev. Discuss., 7, 5661–5698, 2014
www.geosci-model-dev-discuss.net/7/5661/2014/
doi:10.5194/gmdd-7-5661-2014


Geoscientific Model Development Discussions
Open Access



# NEMO-ICB (v1.0): interactive icebergs in the NEMO ocean model globally configured at coarse and eddy-permitting resolution

**R. Marsh[1], V. O. Ivchenko[1], N. Skliris[1], S. Alderson[2], G. R. Bigg[3], G. Madec[2,4], A. Blaker[2], and Y. Aksenov[2]**

[1]University of Southampton, National Oceanography Centre, Southampton, UK
[2]National Oceanography Centre, Southampton, UK
[3]Department of Geography, University of Sheffield, Sheffield, UK
[4]LOCEAN-IPSL, CNRS-IRD-UPMC-MNHN, Paris, France

Received: 23 June 2014 – Accepted: 8 August 2014 – Published: 25 August 2014

Correspondence to: R. Marsh (rm12@soton.ac.uk)

Published by Copernicus Publications on behalf of the European Geosciences Union.







## Abstract

NEMO-ICB features interactive icebergs in the NEMO ocean model. Simulations with coarse (2°) and eddy-permitting (0.25°) global configurations of NEMO-ICB are undertaken to evaluate the influence of icebergs on sea-ice, hydrography and transports, through comparison with control simulations in which the equivalent iceberg mass flux is applied as coastal runoff, the default forcing in NEMO. Comparing a short (14 year) spin-up of the 0.25° model with a computationally cheaper 105 year spin-up of the 2° configuration, calving, drift and melting of icebergs is evidently near equilibrium in the shorter simulation, justifying closer examination of iceberg influences in the eddy-permitting configuration. Freshwater forcing due to iceberg melt is most pronounced in southern high latitudes, where it is locally dominant over precipitation. Sea ice concentration and thickness in the Southern Ocean are locally increased with icebergs, by up to ∼ 8 and ∼ 25 % respectively. Iceberg melting reduces surface salinity by ∼ 0.2 psu around much of Antarctica, with compensating increases immediately adjacent to Antarctica, where coastal runoff is suppressed. Discernible effects on salinity and temperature extend to 1000 m. At many locations and levels, freshening and cooling indicate a degree of density compensation. However, freshening is a dominant influence on upper ocean density gradients across much of the high-latitude Southern Ocean, leading to weaker meridional density gradients, a reduced eastward transport tendency, and hence an increase of ∼ 20 % in westward transport of the Antarctic Coastal Current.

## 1 Introduction

Fresh water fluxes from the terrestrial cryosphere comprise liquid runoff and calved icebergs. This partitioning is believed to be significant for freshwater distribution in the oceans (Gladstone et al., 2001). Runoff freshens the ocean locally near the coast,





GMDD
7, 5661–5698, 2014



while individual icebergs represent pathways for continuous and increasingly remote freshwater influence on the open ocean (Bigg et al., 1996, 1997).

In order to accommodate the climatic influence of icebergs, principally through the freshwater input to the ocean, it is necessary to model their statistical distribution, rather than track large numbers of individual bergs (Hunke and Comeau, 2011). Interactive ocean-iceberg modelling began with the development of an ocean-forced iceberg trajectory model that includes drag forces from ocean, wind, waves and sea-ice, Coriolis and pressure gradient forces to drive the icebergs, and mass loss terms due to basal melting, buoyant convection, and wave erosion (Bigg et al., 1996). This model has been extensively used and validated in the Arctic (e.g. Bigg et al., 1996) and Antarctic (Gladstone et al., 2001), as well as for palaeoclimate studies (e.g. Watkins et al., 2007).

The iceberg model was subsequently coupled with the ocean model FRUGAL, which features a curvilinear grid system with a North Pole centred in Greenland, ensuring reasonably high resolution (20–50 km) in the northern Atlantic and Arctic (Wadley and Bigg, 2000). This coupling allows for feedback between iceberg meltwater and the surface ocean dynamics and thermodynamics (Levine and Bigg, 2008). For a given calving flux, a distribution of icebergs is specified in terms of size, with characteristic length, width and thickness.

In separate developments, modified versions of the Bigg et al. (1996, 1997) iceberg model have been coupled with the ECBilt-CLIO Earth System Model (Jongma et al., 2009) and the CM2G climate model (Martin and Adcroft, 2010). Jongma et al. (2009) found that freshening and cooling influences of icebergs enhance sea-ice area by 12 and 6 % respectively. Martin and Adcroft (2010) conversely found that sea-ice cover is thinner and less compact with icebergs, compared to a control experiment in which fresh water enters the ocean at the coast and stimulates sea-ice growth. They found strongest decreases in sea-ice concentration of 6–8 % in the Amundsen, Bellingshausen, Weddell, and D'Urville Seas, i.e., along the major export routes for icebergs. The reduced fresh-water input over continental shelf regions in experiments with icebergs (in particular, the flux of "bergy bits") enhances deep-water formation in CM2G –





GMDD
7, 5661–5698, 2014



a next-generation GFDL climate model, featuring an isopycnal-coordinate ocean component – leading to an increase in AABW production of up to 10 %.

In the present study, a modified version of the Bigg et al. (1996, 1997) iceberg model, developed by Martin and Adcroft (2010), is coupled to an eddy-permitting global implementation of NEMO (Madec, 2008), to stimulate the trajectories and melting of calved icebergs from Antarctica and Greenland in the presence of mesoscale variability and fine-scale dynamical structure. The rest of the paper is organised as follows. In a model description section, details of NEMO configuration, the iceberg module, implementation, calving and diagnostics are provided. In a model validation section, we consider first the distribution of icebergs and the associated freshwater flux, followed by differences, attributed to the inclusion of icebergs, in sea-ice, hydrography and regional circulation around Antarctica. In a summary and discussion section, we compare and contrast our present results with observations and previous simulations, before highlighting some caveats related to physical processes that are yet to be included in coupled iceberg-ocean models. We conclude with details of code availability.

## 2 Model description

### 2.1 NEMO version and configuration

Iceberg coupling is implemented in the "nemo_v3_5_beta" version of NEMO, in a model option known as NEMO-ICB (see http://www.nemo-ocean.eu/About-NEMO/News/New-release-of-2012-developments), to be released in NEMO v3.6. The source code and forcing files used in the configurations presented here are available to registered NEMO users (see Sect. "Code availability"). The NEMO ocean model component is coupled to the Louvain-la-Neuve sea-ice model LIM2 with viscous-plastic rheology, formulated by Fichefet and Maqueda (1997). The model has been updated by Timmermann et al. (2005), configured and tuned for use in high-resolution configurations (e.g., Johnson et al., 2012).





GMDD
7, 5661–5698, 2014



The performance of the present configuration of NEMO has been evaluated against available observations and compared to the other widely used sea-ice–ocean models in the framework of the Arctic Ocean Intercomparison Project (AOMIP, Proshutinsky et al., 2011). The comparison shows a good agreement with observed fields in the Arctic and subarctic seas, such as sea-ice concentration and thickness, mixed layer depth, and with observed oceanic fluxes through the key straits connecting the Arctic Ocean to the World Ocean (Jahn et al., 2012; Johnson et al., 2012). The model also has been validated in the Atlantic Ocean (Grist et al., 2010) and globally (Megann et al., 2014).

In a development phase, the iceberg model was implemented and tested in a global version of NEMO at 2° resolution (ORCA2), in 105 year experiments forced with a climatological annual cycle derived from the CORE forcing dataset (Large and Yeager, 2004). We subsequently run shorter 14 year experiments at 0.25° resolution (ORCA025). We henceforth refer to corresponding NEMO experiments as "CONTROL", and NEMO-ICB experiments as "ICEBERG".

### 2.2 Iceberg model

The iceberg module is based on the original model of Bigg et al. (1997), as recently adapted for coupling to the CM2G climate model by Martin and Adcroft (2010). Icebergs are treated as Lagrangian particles, with the distribution of icebergs by size derived from observations (see Bigg et al., 1997, and Table 1). The momentum balance for icebergs is comprised of the Coriolis force, air and water form drags, the horizontal pressure gradient force, a wave radiation force, and interaction with sea-ice. The mass balance for an individual iceberg is governed by basal melting, buoyant convection at the side-walls, and wave erosion (see Bigg et al., 1997). All respective equations are the same as detailed in Martin and Adcroft (2010), so are not repeated here.

Internal stresses from the sea-ice model are not used in the iceberg momentum balance, and similarly there is no feedback from the iceberg motion to the sea-ice. Neglect of the momentum exchange between icebergs and sea-ice is consistent with





GMDD
7, 5661–5698, 2014



resolved length scales. The length scale of our biggest represented icebergs is ∼ 1 km, and such icebergs are generally well dispersed around Antarctica and Greenland. Only near release sites will there be a sufficient iceberg density to perhaps impact sea-ice motion, which is determined on model grid scales that are more than ten times larger than our largest icebergs. Independent of iceberg concentration, the impact of sea-ice drag on icebergs is observed to be minimal around 80–90 % of the time (Lighey and Hellmer, 2001), so the momentum interaction term, and any resulting feedback, may be regarded as second order. Only when the pack is concentrated does this change, and then there is a switch to the berg being carried by the sea-ice. This step change in iceberg dynamics is not yet parameterized. We also assume a given orientation for the iceberg relative to the wind. This may or may not be the case in reality. Thus, any stress provided from the sea-ice model grid is likely to only be approximate. For all these reasons, a simple drag law is realistic for iceberg interaction with sea-ice. For higher resolution ocean models, with grid-cell dimensions of just a few km, it would be necessary to more explicitly account for momentum transfers between icebergs and sea-ice, but the present resolution prohibits such representation.

Sea ice concentration and thickness can also be impacted by freshwater fluxes from melting. Given the scale issues mentioned above, but the spreading of meltwater widely across the surface, one can argue that the effect of meltwater on these sea-ice parameters is likely to be much greater than the imprecisely represented and resolved dynamical effect.

### 2.3 Model implementation

The iceberg module is here included directly in the ocean module, independent of the sea-ice model used in NEMO. This is in contrast to the implementation of Martin and Adcroft (2010), who included the iceberg model as part of the sea-ice module of CM2G, requiring that the iceberg module be re-coded if an alternative sea-ice model is used. Furthermore, icebergs in the real world are largely submerged into the ocean, and therefore influenced by vertical temperature gradients and current shears.





GMDD
7, 5661–5698, 2014



For physically correct model representation of iceberg-ocean coupling, model icebergs should correspondingly be submerged in the model ocean – difficult to code within the CM2G scheme. Although submerged icebergs are not yet represented in NEMO-ICB, the development of such fidelity in the coupling should be straightforward by contrast, as the dynamics and thermodynamics routines (see Sect. “Code availability”) can be extended to 3-D settings with only minor changes to the existing modules.

### 2.4 Calving

Approximately climatological iceberg calving rates are distributed realistically around Greenland and Antarctica (as shown in Fig. 2a of Levine and Bigg, 2008), and the implied calving events are constant through time. The initial length/width ratio for all newly calved icebergs is 1.5, and size distributions are as listed in Table 1. Annual-mean calving around Antarctica is specified at the rate of 1140 Gt year$^{-1}$, compared to 1332 Gt year$^{-1}$ in Gladstone et al. (2001) and 1375 Gt year$^{-1}$ in Levine and Bigg (2008) – from 1500 km$^3$ year$^{-1}$ in the latter study, taking density of ice at 0 °C as 916.7 kg m$^{-3}$. The Antarctic calving rate comprises about two thirds of total freshwater flux into the Southern Ocean from Antarctica (1700 Gt year$^{-1}$). The mean calving rate in the Northern Hemisphere is considerably smaller, $\sim$ 183 Gt year$^{-1}$, compared to 206 Gt year$^{-1}$ (from 225 km$^3$ year$^{-1}$) in Levine and Bigg (2008). The Greenland calving rate comprises around 50 % of total freshwater flux into the North Atlantic from Greenland.

We note here that our calving rates may be somewhat conservative in the context of ongoing changes. The original calving rate estimates used in Gladstone et al. (2001) and Levine and Bigg (2008), for example, used approaches taken before the satellite era. Rignot et al. (2011) report steadily increasing rates of ice discharge (remote sensing of ice motion and thickness) over 1992–2009, $\sim$ 500 to $\sim$ 630 Gt year$^{-1}$ for Greenland, and $\sim$ 2140 to $\sim$ 2300 Gt year$^{-1}$ for Antarctica. The partitioning of this discharge between calving and melting (basal melting of outlet glaciers and ice shelves) is poorly known and undoubtedly changing rapidly, but it is likely that recent calving rates are substantially higher than those used to develop earlier climatological rates, and





GMDD
7, 5661–5698, 2014



trending upwards. The oceanographic and sea-ice impacts reported here are therefore also likely to be conservative.

### 2.5 Diagnostics

For a given time interval, the locations and properties of individual iceberg particles (each representative of varying numbers of icebergs in a given class – see Table 1) are saved in a set of files that may be post-processed to obtain selected distributions and tracks for individual icebergs.

Integral diagnostics are written to the tracer files of standard NEMO output. Table 2 lists the full suite of these diagnostics, along with corresponding variable names and units. Most diagnostics are 2-D fields on the NEMO ocean model mesh. Particularly useful instantaneous measures of the iceberg model are the virtual coverage by icebergs and the melt rate of icebergs, in total and partitioned into the three components: "buoyancy component of iceberg melt rate" (basal melting); "convective component . . . " (sidewall melting); "erosion component . . . " (wave erosion).

## 3 Model evaluation

We first consider the spin-up of NEMO-ICB at both 0.25° and 2° resolutions, in terms of total iceberg volume. We then illustrate typical near-equilibrium iceberg distributions, based on year 10–14 averages, for both configurations. We subsequently examine sea-ice concentration and thickness, hydrography, and – for the eddy-permitting configuration only – iceberg influences on the regional circulation around Antarctica.

### 3.1 Iceberg distribution and freshwater flux

Time series of the total mass of icebergs (Fig. 1) indicate that Southern Hemisphere (SH) calving and melting rates are in near balance by 10 years in ORCA2, but a further ∼ 50 years is needed for global balance, due to slower equilibration in the Northern





GMDD
7, 5661–5698, 2014



Hemisphere (NH). A similar fast SH equilibration is apparent in ORCA025, with NH ice mass still increasing at year 14. The NH iceberg mass equilibrates more slowly due to the prevalence of semi-enclosed basins in the NH compared to the SH, which extends the lifetimes of the NH icebergs. It therefore requires some time for the mean iceberg mass of the Arctic in particular, but also Baffin Bay, to reach equilibrium.

In ORCA2 after 100 years, iceberg mass in the SH exceeds that in the NH by ∼ 40 %. This excess is considerably less than the factor of 6 difference in calving rates between Hemispheres. The storage of icebergs within the more complex geography of the NH, combined with the rapid melting in the SH of icebergs that move into warmer waters equatorwards from the Coastal Current is likely to be responsible for this lessening in contrast between the NH and SH. However, the model does not include giant icebergs, of which there will always be some in the Southern Ocean (Silva et al., 2006) and which will take much longer to melt. The real ratio of iceberg mass between the Hemispheres is therefore likely to be greater than in the model. The ORCA2 (year 100) global iceberg mass of 1200 Gt is considerably lower than the ∼ 6000 Gt obtained after 100 years spin-up of CM2G (Martin and Adcroft, 2010), although SH ice mass totals of ∼ 700 Gt (ORCA2) and ∼ 600 Gt (ORCA025) are more consistent with estimates of iceberg mass in the Southern Ocean (equatorward of 66° S) – based on satellite observations – seasonally varying in the range 0–500 Gt during 2002–10 (Tournadre et al., 2012). As further discussed below, the high global iceberg mass in CM2G is associated with excessive calving rates in the Pacific sector of Antarctica (see Fig. 9a in Martin and Adcroft, 2010).

Global iceberg mass budgets for NEMO-ICB (ORCA2 and ORCA025) and CM2G are summarized in Table 3. We note that NEMO-ICB is further from steady state than CM2G, although this may be a consequence of fixing the global calving rate in our case. We further note, with ORCA2, a transition from positive to negative net fluxes, comparing early and late stages in the simulation. This is related to slow adjustment of the iceberg mass balance in the North Atlantic. Wave erosion is clearly dominant in both models, while buoyant convection is negligible. Bigg et al. (1997) note similar





GMDD
7, 5661–5698, 2014



magnitudes and partitioning in the North Atlantic and Arctic, although a later version of the model featured enhanced basal melting (Gladstone et al., 2001).

We might expect more difference in partitioning between the North Atlantic, dominated by wave erosion, and the Arctic, where basal melting should be enhanced in the presence of a relatively warm Atlantic layer (at around 100 m in many places). However, surface temperatures are used in the basal melting parameterization of NEMO-ICB, which may limit basal melting in the Arctic, where surface temperatures are close to the freezing point during most of the year. In spite of the adopting the same parameterizations as Martin and Adcroft (2010), we obtain somewhat different global rates and partitioning (see Table 3). While wave erosion flux is still dominant in CM2G, accounting for 70 %, basal melt flux is more substantial. Sidewall melting is similarly negligible.

With respect to the Southern Hemisphere that we focus on below, in the ORCA025 configuration of NEMO-ICB, total melting of icebergs from Antarctica (dominating the global budget) averaged over years 10–14 is 1126.8 Gt year$^{-1}$. This almost exactly balances total Antarctic calving of 1131.7 Gt year$^{-1}$, whereas there is a higher imbalance in the *global* case (see Table 3), attributed to slower equilibration in the Northern Hemisphere. For years 10–14, we partition SH iceberg mass loss as follows: wave erosion of 955.7 Gt year$^{-1}$ (84.81 % of the total); basal melting of 163.9 Gt year$^{-1}$ (14.55 %); sidewall melting of 7.23 Gt year$^{-1}$ (0.64 %).

As an example of simulated iceberg distributions, Fig. 2 shows end of year 14 instantaneous locations of individual icebergs (colour-coded by thickness) in ORCA025 and ORCA2, for SH and NH separately. In SH, large icebergs (thickness > 200 m) cluster along most of the Antarctic coast in both experiments, with smaller icebergs (thickness < 50 m) found farther offshore in the Southern Ocean. In both ORCA025 and ORCA2, icebergs are spread further equatorward in three sectors: in the north part of the Weddell Gyre (east of the Antarctic peninsula to about 20° E), in the Indian Ocean sector (60–120° E), and south of Australia (around 180° W). Icebergs may initially drift northwards due to topographically induced distortions of the coastal current, subsequently





GMDD
7, 5661–5698, 2014



following the periphery of subpolar gyres to reach the Antarctic Circumpolar Current, where they melt rapidly.

In the NH, highest iceberg concentrations are located to the west of Greenland, in Nares Strait and Baffin Bay, and north of Greenland and around Ellesmere island. The majority of the icebergs follow the Labrador Current and are fully melted within the vicinity of the Grand Banks. While broadly similar, we note systematic differences between ORCA025 and ORCA2. Overall, icebergs are more randomly dispersed in ORCA025, as would be expected at eddy-permitting resolution, while large icebergs have drifted further north in the Southern Ocean, and further away from Greenland, in ORCA2. The distributions in Fig. 2 are partly related to the time of the year, as fewer (more) icebergs would be expected in the North Atlantic (Southern Ocean) at the end of December because of contrasting melting rates over the previous few months.

Figure 3 shows spatial distributions of the total freshwater fluxes due to iceberg melting, averaged over years 10–14, while Fig. 4 shows these fluxes as fractions of the net freshwater flux associated with local imbalances of precipitation and evaporation (P–E). The absolute fluxes are broadly similar in both ORCA025 and ORCA2, although some differences are notable (Fig. 3). High melt rates are more confined close to Antarctica in ORCA025, while traces of weak melt rates reach lower latitudes in the southwest Atlantic. High melt rates that are prevalent in the southern Weddell Sea of ORCA2 are absent in ORCA025.

As a fraction of P–E, iceberg melting exceeds 1.0 at many locations (Fig. 4), and differences are again apparent between ORCA025 and ORCA2. This is in contrast to the findings of Martin of Adcroft (2010) that "... iceberg melt water rarely accounts for more than 10 % of the total fresh-water input to the open ocean ...", consistent with the location of most melting closer to Antarctica in CM2G, where the freshwater flux associated with sea-ice melt dominates total freshwater flux (see Figs. 2a and 10 in Martin and Adcroft, 2010).

In the southwest Greenland Sea of ORCA2, iceberg melting as a fraction of net freshwater flux is negative as the net freshwater flux is locally reversed where sea-ice





GMDD
7, 5661–5698, 2014
NEMO-ICB (v1.0)
R. Marsh et al.



formation acts to increase salinity (not shown), although both terms are locally small. More dominant iceberg melting is evident close to the Falklands in ORCA025. Both melting patterns (and amplitudes) bear favourable comparison with estimates based on satellite observations (Tournadre et al., 2012).

### 3.2 Sea ice changes

Icebergs influence sea-ice distribution, thickness and total mass. In both ORCA025 and ORCA2, the inclusion of icebergs leads to more seasonally persistent and thicker sea-ice, in both hemispheres. These changes are most evident in the SH. Figures 5 and 6 show year 10–14 means for ICEBERG and ICEBERG minus CONTROL differences in sea-ice concentration and thickness, for both ORCA025 and ORCA2.

The total mass of sea-ice (averaged over years 10–14) of $3.46 \times 10^{15}$ kg in CONTROL is increased by 4 % in ICEBERG. Following the energy budget of Martin and Adcroft (2010), we take the latent heat of fusion of water ($334 \times 10^3$ J kg$^{-1}$), and consider a notional SH sea-ice area of $10^{13}$ m$^2$. The sea-ice volume increase in ICEBERG, interpreted as a consequence of differences in the annual cycle compared to CONTROL, thus equates to a reduced energy uptake of 3.66 W m$^{-2}$, similar to the top-of-atmosphere radiative forcing under doubled $CO_2$.

With sea-ice concentration close to 1.0 over large areas of the Weddell and Ross Seas (Fig. 5), the effect of icebergs is small, with changes in the range ±1 %. In the Indian and western Pacific sectors, between 60° E and 150° W, differences reach +8 % in the zone 65–70° S, where CONTROL sea-ice concentrations are lower. In ORCA025 only, negative values of up to −3 % are evident locally in the Bellingshausen and Amundsen Seas, and along the western Antarctic Peninsula.

With sea-ice thickness largely in the range 0–100 cm for CONTROL, ICEBERG minus CONTROL differences mostly lie in the range −2 cm to +10 cm, with increases far more commonplace. Thickness is locally increased by up to ∼ 25 % in ICEBERG compared to CONTROL. In most areas, changes of sea-ice thickness (Fig. 6) are coincident with changes in concentration, suggesting a dynamical effect of icebergs on sea-ice.





GMDD
7, 5661–5698, 2014



We infer that the presence of icebergs increases sea-ice convergence in the western Weddell Sea, towards the Antarctic Peninsula, and in the northern Ross Sea. In the Bellingshausen and Amundsen Seas of ORCA025, sea-ice drift is westward along the shore and divergent (e.g., Holland and Kwok, 2012). In these regions, icebergs thus appear to increase the divergence of sea-ice transport, conversely decreasing ice thickness and concentration.

Increased sea-ice concentration/thickness in ICEBERG contrasts with decreases at most affected grid-points in the coupled atmosphere–ocean model of Martin and Adcroft (2010). The distribution of sea-ice concentration in CONTROL is also considerably different from that in the CTRL experiment of Martin and Adcroft (2010) – see their Fig. 4a – with higher concentrations and greater equatorward extent in both ORCA025 and ORCA2. In the Greenland/Arctic area, the presence of icebergs lead to only minor redistributions of sea-ice concentration and thickness (not shown).

### 3.3 Hydrographic impacts

Figures 7–10 show differences at four selected depth levels in salinity (left panels) and temperature (right panels), between ICEBERG and CONTROL experiments. The hydrographic impact of melting icebergs is most directly evident in surface salinity (Fig. 7). Differences are positive immediately adjacent to Antarctica, where runoff is substantially reduced (in proportion to the specified calving flux). Negative differences are more dominant at the surface just offshore, extending far to the north in the Southern Ocean, generally coincident with positive sea-ice concentration and thickness anomalies.

With increasing depth, extensive belts of positive salinity difference are encountered. At 159 m, positive differences are most prominent in ORCA025 to the south of Australia and in the northern Weddell Sea (Fig. 8). By 511 m (Fig. 9), positive anomalies dominate the region south of $\sim 50^{\circ}$ S. At 1033 m (Fig. 10), negative anomalies are even more limited in extent. Salinity anomalies in the NH are by contrast considerably smaller.

Temperature differences between ICEBERG and CONTROL are small at the surface (Fig. 7) relative to sub-surface (Figs. 8–10), but with quite different patterns in





GMDD
7, 5661–5698, 2014
NEMO-ICB (v1.0)
R. Marsh et al.



ORCA025 compared to ORCA2. Largest negative surface differences are located in the west Pacific sector of ORCA025, compared to the Weddell Sea of ORCA2 (both early and late in that simulation). At 159 m, the inclusion of icebergs in ORCA025 promotes strong warming (up to 0.5 °C over wide areas) throughout much of the Weddell Sea, and from the eastern Indian sector to the western Pacific sector, in contrast to strong cooling adjacent to much of Antarctica and more moderate equatorward warming in ORCA2 (Fig. 8). By 511 m, icebergs promote extensive Southern Ocean warming in ORCA025 and ORCA2 (Fig. 9). By 1033 m, this warming is stronger in ORCA2 than in ORCA025, and becomes more extensive later in the ORCA2 simulation (Fig. 10).

Differences between ICEBERG and CONTROL in the Southern Ocean should be appreciated alongside historical changes. Upper ocean salinity differences shown in Figs. 7 and 8 are comparable to observed 50 year trends in the Southern Ocean that range $\pm 0.2\,\mathrm{psu}\,(50\,\mathrm{yr})^{-1}$ (Durack and Wijffels, 2010). Deep temperature differences between ICEBERG and CONTROL in Figs. 9 and 10 are comparable to observed decadal changes in the Southern Ocean below 1000 m, where trends in the range 0.02–0.04 °C decade$^{-1}$ are estimated over the 1990s and 2000s (Purkey and Johnson, 2010). A substantial increase of the Antarctic iceberg flux over recent decades could account for some of the observed changes, although the hemispheric iceberg record necessary to investigate such a possibility has only been available from 2001 (Tournadre et al., 2012), and observations for the 60–150° E sector indicate no clear trends in iceberg volume over 1983–2000 (Jacka and Giles, 2007).

Substantial temperature differences are also evident in equatorial zones of the Atlantic and Pacific, and the western boundary currents. The rapid appearance of differences in locations remote from the polar latitudes is consistent with wave-like propagation of signals from the regions directly impacted by icebergs. The mechanism for such a quick response likely involves the propagation of planetary Kelvin and Rossby waves, which most clearly disturb the more energetic currents, as shown by Atkinson et al. (2009).





GMDD
7, 5661–5698, 2014
NEMO-ICB (v1.0)
R. Marsh et al.



To show how temperature and salinity change in relation to density for selected regions where iceberg influences are strongest, Figs. 11 and 12 show $T$–$S$ diagrams for all grid points, and area-averaged, in the Ross Sea/Pacific and Weddell Sea/Atlantic sectors (both south of 60° S). An overall impression (upper panels) is that ICEBERG salinities (red points) are mostly shifted to lower salinity, by up to 0.1 psu relative to CONTROL salinities (blue points). Area-averaged differences are generally not temperature-compensated, leading to density reductions (shifts across isopycnals) on depth levels in the upper 1000 m (lower panels), reaching maxima of $\sim 0.05\,\mathrm{kg\,m^{-3}}$ and $\sim 0.1\,\mathrm{kg\,m^{-3}}$ at the surface, in the Ross Sea and Weddell Sea respectively. Below $\sim 1000$ m, changes of salinity and temperature are very close to density-compensating, although there are, on average, slight density increases in ICEBERG at around 3000 m in the Ross Sea (Fig. 11) and at around 2500 m in the Weddell Sea (Fig. 12).

### 3.4 Dynamical impacts

Noting the substantial reductions of surface density in the Ross and Weddell sectors, we investigate how icebergs alter the horizontal distribution of density in the upper ocean around Antarctica in ORCA025. The year 10–14 mean potential density anomaly, $\sigma_0$, in ICEBERG illustrates highest surface densities around Antarctica, with maxima of $\sim 27.9\,\mathrm{kg\,m^{-3}}$ in the Pacific sector (Fig. 13, upper panel). A notable feature is the ribbon of lower density, in the range 27.0–27.5 $\mathrm{kg\,m^{-3}}$, typically around 0.25 $\mathrm{kg\,m^{-3}}$ below values immediately offshore. Differences in Fig. 13 (lower panel) are dominated by negative values (minima exceeding $-0.1\,\mathrm{kg\,m^{-3}}$), associated with surface freshening due to melting icebergs, and a band of positive differences around much of coastal Antarctica, where differences at many coastal grid-points exceed $0.1\,\mathrm{kg\,m^{-3}}$, associated with the strongly reduced runoff in ICEBERG.

In combination, differences in the distribution of surface density around Antarctica amount to a reduction in ICEBERG of the cross-shelf density gradient that drives an eastward flow component via the thermal wind balance (Núñez-Riboni and Fahrbach, 2009, 2010). Near-coastal transport is otherwise westward: located on the slope





GMDD
7, 5661–5698, 2014
NEMO-ICB (v1.0)
R. Marsh et al.



between the shelf waters and the Southern Ocean is the Antarctic Coastal Current (ACoC), which is primarily wind-driven (Hayakawa et al., 2012). We might therefore expect a stronger ACoC in ICEBERG due to a reduction in the thermal wind component that otherwise opposes the (unchanged) wind-driven transport. This is indeed the case. Figure 14 (upper panel) shows the year 10–14 mean barotropic streamfunction in ICEBERG, illustrating the existence of a circumpolar Antarctic Coastal Current (ACoC) that transports ∼ 8.5 Sv to the west, located south of an Antarctic Circumpolar Current that transports ∼ 130 Sv to the east. Differences relative to CONTROL (Fig. 14, lower panel) feature a coherent circumpolar band of anomalies around −1.5 Sv (i.e., a weaker ACoC in CONTROL transports ∼ 7 Sv) – i.e., in the presence of icebergs, the ACoC is strengthened by ∼ 20 %.

The meridional overturning circulation (MOC) is little affected by the inclusion of icebergs. In the Antarctic Zone to south of 65° S, ICEBERG minus CONTROL differences in the MOC streamfunction are persistently negative, with largest differences around −0.2 Sv in the depth range 500–1500 m (not shown), representing 10 % intensification of the overturning adjacent to Antarctica. In a longer simulation, such differences may further evolve, associated with changes in bottom water formation.

## 4 Summary and discussion

We have included icebergs interactively in an eddy-permitting global configuration of NEMO, the first time that icebergs have been implemented at this resolution. Icebergs are most extensive and influential in the Southern Ocean. Simulated iceberg distributions and freshwater fluxes are in reasonable agreement with observations. Sea ice concentration and thickness around Antarctica are increased by up to 8 and 25 % respectively if icebergs are included in NEMO. Strong freshening of the upper ocean is only partly compensated by temperature changes, leading to widespread reductions of density, except in a narrow coastal zone where the re-allocation of runoff to iceberg calving results in increased density. The net effect is a reduction of horizontal





GMDD
7, 5661–5698, 2014
NEMO-ICB (v1.0)
R. Marsh et al.



pressure gradients around much of Antarctica, strengthening westward coastal transport by around 20 % through suppression of the buoyancy-driven eastward transport that opposes wind-driven westward transport.

Regarding prospects for future experiments and model development, NEMO-ICB may be used in CMIP6 experiments. The present representation of icebergs excludes more subtle interactions with the ocean. Simulated icebergs presently drift with the surface current. We plan to specify drift with depth-averaged currents to more accurately track icebergs in regions of strong vertical shear. Icebergs may also exert a more remote influence on hydrography, at distances of up to several 10's of km (Stephenson et al., 2011). Melting at sufficient depth will lead to the entrainment and upwelling of relatively warm and salty Circumpolar Deep Water around large icebergs in the Southern Ocean (Jenkins, 1999). Stephenson et al. (2011) report observations of the corresponding alternative ways that ice meltwater disperses from a large tabular iceberg in the northern Weddell Sea: turbulent entrainment, localized near the berg; wider horizontal dispersal due to double diffusive processes, a process originally demonstrated in pioneering laboratory experiments (Huppert and Turner, 1980). Parameterization of these processes may further improve the realism of melting rates, and hence the simulated distribution of icebergs in the World Ocean.

## Code availability

NEMO-ICB is available via the NEMO home page, where new users can register via http://www.nemo-ocean.eu/user/register. Registered users can access the ICB modules at: https://forge.ipsl.jussieu.fr/nemo/browser#trunk/NEMOGCM/NEMO/OPA_SRC/ICB.

ICB comprises the following modules:

icb_oce.F90 – declares variables for iceberg tracking

icbclv.F90 – calving routines for iceberg calving





GMDD
7, 5661–5698, 2014



icbdia.F90 – initialises variables for iceberg budgets and diagnostics

icbdyn.F90 – time stepping routine for iceberg tracking

icbini.F90 – initialises variables for iceberg tracking

icblbc.F90 – routines to handle boundary exchanges for icebergs

icbrst.F90 – reads and writes iceberg restart files

icbstp.F90 – initialises variables for iceberg tracking

icbthm.F90 – thermodynamics routines for icebergs

icbtrj.F90 – trajectory I/O routines

icbutl.F90 – various iceberg utility routines

Default iceberg parameters are specified in: https://forge.ipsl.jussieu.fr/nemo/browser/trunk/NEMOGCM/CONFIG/SHARED/namelist_ref.

When compiling NEMO-ICB, the flag ln_icebergs in this namelist file is set to.true.

*Acknowledgements.* We thank Torge Martin and Alistair Adcroft for providing their code as a basis for the icebergs module. Funding to couple NEMO with the icebergs module was provided by the UK Natural Environment Research Council (grant number NE/H021396/1) for the project “a century of variability in Greenland melting and iceberg calving”.

## References

Atkinson, C. P., Wells, N. C., Blaker, A. T., Sinha, B., and Ivchenko, V. O.: Rapid ocean wave teleconnections linking Antarctic sea salinity anomalies to the equatorial ocean–atmosphere system, Geophys. Res. Lett., 36, L08603, doi:10.1029/2008GL036976, 2009.

Bigg, G. R. and Wadley, M. R.: Prediction of iceberg trajectories for the North Atlantic and Arctic Oceans, Geophys. Res. Lett., 23, 3587–3590, 1996.





GMDD

7, 5661–5698, 2014



Bigg, G. R., Wadley, M. R., Stevens, D. P., and Johnson, J. A.: Modelling dynamics and thermodynamics of icebergs, Cold Reg. Sci. Technol., 26, 113–135, 1997.
Durack, P. J. and Wijffels, S. E.: Fifty-year trends in global ocean salinities and their relationship to broad-scale warming, J. Climate, 23, 4342–4362, doi:10.1175/2010JCLI3377.1, 2010.
Fichefet, T. and Maqueda, M. A.: Sensitivity of a global sea-ice model to the treatment of ice thermodynamics and dynamics, J. Geophys. Res., 102, 12609–12646, 1997.
Gladstone, R., Bigg, G. R., and Nicholls, K.: Iceberg trajectory modeling and meltwater injection in the Southern Ocean, J. Geophys. Res., 106, 19903–19915, 2001.
Grist, J. P., Josey, S. A., Marsh, R., Good, S. A., Coward, A. C., de Cuevas, B. A., Alderson, S. G., New, A. L., and Madec, G.: The roles of surface heat flux and ocean heat transport convergence in determining Atlantic Ocean temperature variability, Ocean Dynam., 60, 771–790, doi:10.1007/s10236-010-0292-4, 2010.
Holland, P. R. and Kwok, R.: Wind-driven trends in Antarctic sea-ice drift, Nat. Geosci., 5, 872–875, doi:10.1038/ngeo1627, 2012.
Hunke, E. C. and Comeau, D.: Sea ice and iceberg dynamic interaction, J. Geophys. Res., 116, C05008, doi:10.1029/2010JC006588, 2011.
Huppert, H. E. and Turner, J. S.: Ice blocks melting into a salinity gradient, J. Fluid. Mech., 100, 367–384, 1980.
Jacka, T. H. and Giles, A. B.: Antarctic iceberg distribution and dissolution from ship-based observations, J. Glaciol., 53, 341–356, 2007.
Jahn, A., Aksenov, Y., Cuevas, B. A., Steur, L., Häkkinen, S., Hansen, E., Herbaut, C., Houssais, M.-N., Karcher, M., Kauker, F., Lique, C., Nguyen, A., Pemberton, P., Worthen, D., and Zhang, J.: Arctic Ocean freshwater: how robust are model simulations?, J. Geophys. Res., 117, C00D16, doi:10.1029/2012JC007907, 2012.
Jenkins, A.: The impact of melting ice on ocean waters, J. Phys. Ocean., 29, 2370–2381, 1999.
Johnson, M., Proshutinsky, A., Aksenov, Y., Nguyen, A. T., Lindsay, R., Haas, C., Zhang, J., Diansky, N., Kwok, R., Maslowski, W., Häkkinen, S., Ashik, I., and Cuevas, B. A.: Evaluation of Arctic sea-ice thickness simulated by Arctic Ocean Model Intercomparison Project models, J. Geophys. Res., 117, C00D13, doi:10.1029/2011JC007257, 2012.
Jongma, J. I., Driesschaert, E., Fichefet, T., Goosse, H., and Renssen, H.: The effect of dynamic–thermodynamic icebergs on the Southern Ocean climate in a three-dimensional model, Ocean Model., 26, 104–113, 2009.





GMDD
7, 5661–5698, 2014



Large, W. G. and Yeager, S. G.: Diurnal to Decadal Global Forcing for Ocean and Sea–Ice Models: the Data Sets and Flux Climatologies, Technical Report TN-460+STR, NCAR, 105 pp., 2004.

Levine, R. C. and Bigg, G. R.: The sensitivity of the glacial ocean to Heinrich events from different sources, as modeled by a coupled atmosphere–iceberg–ocean model, Paleoceanography, 23, PA4213, doi:10.1029/2008PA001613, 2008.

Lighey, C. and Hellmer, H. H.: Modeling giant-iceberg drift under the influence of sea-ice in the Weddell Sea, Antarctica, J. Glaciol., 47, 452–60, 2001.

Madec, G.: NEMO Ocean Engine, Note du Pole de modélisation, Institut Pierre-Simon Laplace (IPSL), France, no. 27, 2008.

Martin, T. and Adcroft, A.: Parameterizing the fresh-water flux from land ice to ocean with interactive icebergs in a coupled climate model, Ocean Model., 34, 111–124, 2010.

Megann, A., Storkey, D., Aksenov, Y., Alderson, S., Calvert, D., Graham, T., Hyder, P., Siddorn, J., and Sinha, B.: GO5.0: the joint NERC–Met Office NEMO global ocean model for use in coupled and forced applications, Geosci. Model Dev., 7, 1069–1092, doi:10.5194/gmd-7-1069-2014, 2014.

Proshutinsky, A., Aksenov, Y., Clement-Kinney, J., Gerdes, R., Golubeva, E., Holland, D., Holloway, G., John, A., Johnson, M., Popova, E., Steele, M., and Watanabe, E.: Recent advances in Arctic Ocean studies employing models from the Arctic Ocean Model Intercomparison Project, Oceanography, 24, 102–113, 2011.

Purkey, S. G. and Johnson, G. C.: Warming of global abyssal and deep Southern Ocean waters between the 1990s and 2000s: contributions to global heat and sea level rise budgets, J. Climate, 23, 6336–6351, doi:10.1175/2010JCLI3682.1, 2010.

Rignot, E., Velicogna, I., van der Broeke, M. R., Monaghan, A., and Lenaerts, J.: Acceleration of the contribution of the Greenland and Antarctic ice sheets to sea level rise, Geophys. Res. Lett., 38, L05503, doi:10.1029/2011GL046583, 2011.

Silva, T. A. M., Bigg, G. R., and Nicholls, K. W.: The contribution of giant icebergs to the Southern Ocean freshwater flux, J. Geophys. Res., 111, C03004, doi:10.1029/2004JC002843, 2006.

Stephenson, G. R., Sprintall, J., Gille, S. T., Vernet, M., Helly, J. J., and Kaufmann, R. S.: Subsurface melting of a free-floating Antarctic iceberg, Deep-Sea Res. Pt. II, 58, 1336–1345, doi:10.1016/j.dsr2.2010.11.009, 2011.





GMDD
7, 5661–5698, 2014



Timmermann, R., Goosse, H., Madec, G., Fichefet, T., Ethe, C., and Duliere, V.: On the representation of high latitude processes in the ORCA-LIM global coupled sea-ice–ocean model, Ocean Model., 8, 175–201, doi:10.1016/j.ocemod.2003.12.009, 2005.

Tournadre, J., Girard-Ardhuin, F., and Legrésy, B.: Antarctic icebergs distributions, 2002–2010, J. Geophys. Res., 117, C05004, doi:10.1029/2011JC007441, 2012.

Wadley, M. R. and Bigg, G. R.: Implementation of variable time stepping in an ocean general circulation model, Ocean Model., 1, 71–80, doi:10.1016/S1463-5003(99)00011-6, 2000.

Watkins, S. J., Maher, B. A., and Bigg, G. R.: Ocean circulation at the Last Glacial Maximum: a combined modelling and magnetic proxy-based study, Paleoceanogr., 22, PA2204, doi:10.1029/2006PA001281, 2007.





GMDD
7, 5661–5698, 2014



**Table 1.** Distributions of individual iceberg mass, proportion of calving mass, ratio of effective/real mass (the number of icebergs per Lagrangian particle), and thickness, across the ten classes.

| Iceberg class | Initial mass ($10^7$ kg) | Proportion of calving mass | Ratio between effective and real iceberg mass | thickness of newly calved bergs (m) |
|---|---|---|---|---|
| 1 | 8.8 | 0.24 | 2000 | 40 |
| 2 | 41 | 0.12 | 200 | 67 |
| 3 | 330 | 0.15 | 50 | 133 |
| 4 | 1800 | 0.18 | 20 | 175 |
| 5 | 3800 | 0.12 | 10 | 250 |
| 6 | 7500 | 0.07 | 5 | 250 |
| 7 | 12 000 | 0.03 | 2 | 250 |
| 8 | 22 000 | 0.03 | 1 | 250 |
| 9 | 39 000 | 0.03 | 1 | 250 |
| 10 | 74 000 | 0.02 | 1 | 250 |





GMDD
7, 5661–5698, 2014



**Table 2.** Iceberg integral diagnostics.

| Diagnostic | Variable name | Units |
|---|---|---|
| calving mass input | calving | $kg\,s^{-1}$ |
| calving heat flux | calving_heat | – |
| Melt rate of icebergs + bits | berg_floating_melt | $kg\,m^{-2}\,s^{-1}$ |
| Accumulated ice mass by class | berg_stored_ice | kg |
| Melt rate of icebergs | berg_melt | $kg\,m^{-2}\,s^{-1}$ |
| Buoyancy component of iceberg melt rate | berg_buoy_melt | $kg\,m^{-2}\,s^{-1}$ |
| Erosion component of iceberg melt rate | berg_eros_melt | $kg\,m^{-2}\,s^{-1}$ |
| Convective component of iceberg melt rate | berg_conv_melt | $kg\,m^{-2}\,s^{-1}$ |
| Virtual coverage by icebergs | berg_virtual_area | $m^2$ |
| Mass source of bergy bits | bits_src | $kg\,m^{-2}\,s^{-1}$ |
| Melt rate of bergy bits | bits_melt | $kg\,m^{-2}\,s^{-1}$ |
| Bergy bit density field | bits_mass | $kg\,m^{-2}\,s^{-1}$ |
| Iceberg density field | berg_mass | $kg\,m^{-2}\,s^{-1}$ |
| Calving into iceberg class | berg_real_calving | $kg\,s^{-1}$ |





GMDD
7, 5661–5698, 2014



**Table 3.** Global iceberg mass balances in CM2G and NEMO-ICB.

| Fluxes (Gt year$^{-1}$) | | CM2G* | NEMO-ICB | | |
|---|---|---|---|---|---|
| | | | ORCA025 y10–14 | ORCA2 y10–14 | ORCA2 y101–105 |
| Total fluxes | calving | 2210 | 1303 | 1327.9 | 1327.9 |
| | melting | 2214.3 | 1284.6 | 1303.1 | 1356.4 |
| Net flux (calving – melting) | | −4.3 | +18.4 | +24.8 | −28.5 |
| Components of melt flux (and % contribution) | wave erosion | 1550 (70.0 %) | 1077.9 (83.91 %) | 1121.4 (86.06 %) | 1174.6 (86.60 %) |
| | basal melting | 646.8 (29.21 %) | 198.2 (15.43 %) | 164.9 (12.65 %) | 165.5 (12.20 %) |
| | sidewall melting | 17.5 (0.79 %) | 8.5 (0.66 %) | 16.8 (1.29 %) | 16.3 (1.20 %) |

* Martin and Adcroft (2010)





GMDD
7, 5661–5698, 2014



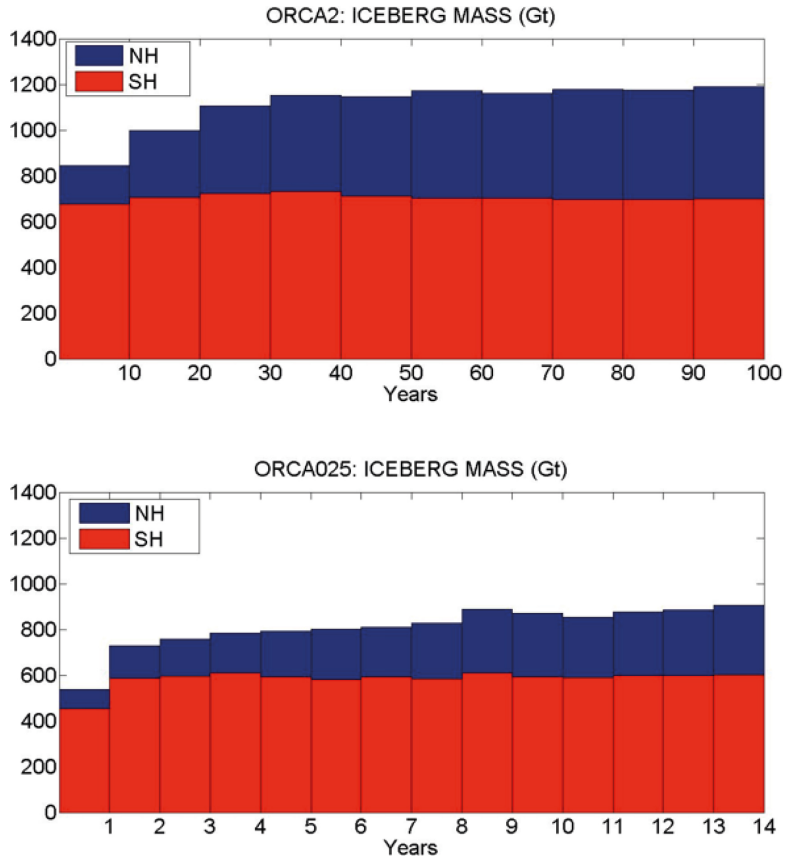


**Figure 1.** Time series of total iceberg mass (1 Gt = $10^9$ t = $10^{12}$ kg): upper panel – ORCA2 (to year 105); lower panel – ORCA025 (to year 14). Southern Hemisphere (SH) iceberg mass is indicated by red bars. Northern Hemisphere (NH) iceberg mass is indicated by blue bars.





GMDD
7, 5661–5698, 2014



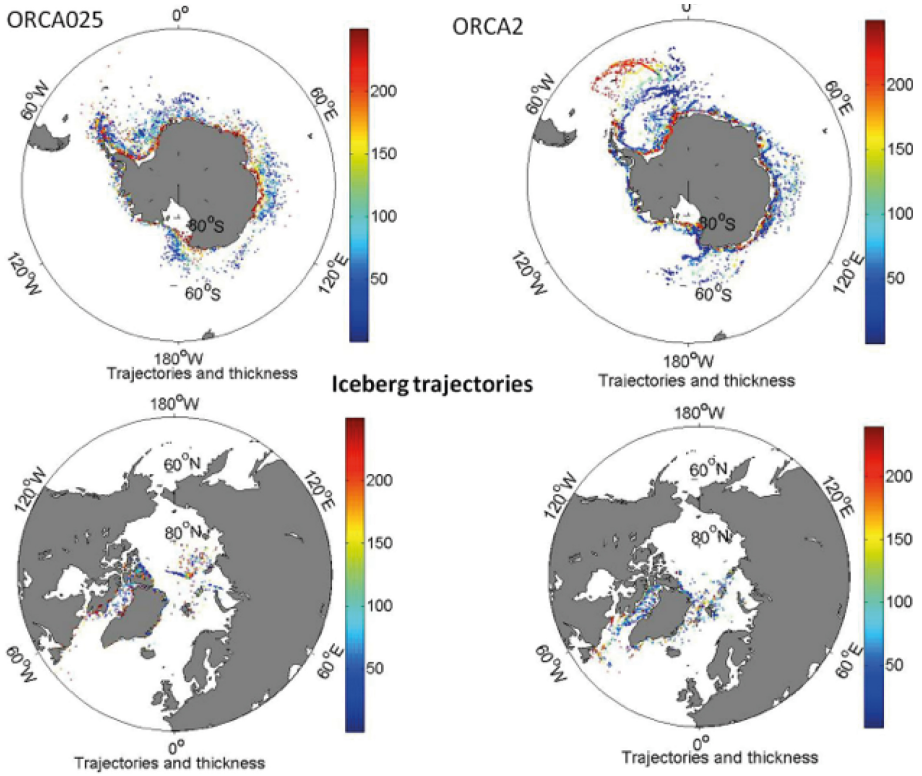


**Figure 2.** Example iceberg locations (end year 14, colour-coded for size class, or thickness): ORCA025 SH (upper left); ORCA2 SH (upper right); ORCA025 NH (lower left); ORCA2 NH (lower right).





GMDD
7, 5661–5698, 2014
NEMO-ICB (v1.0)
R. Marsh et al.



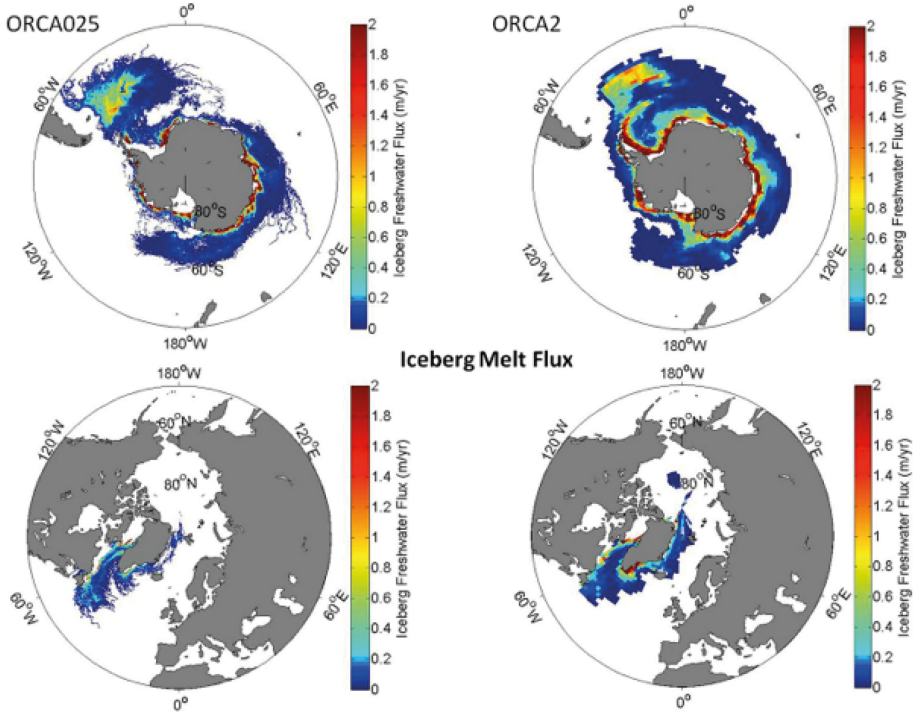


**Figure 3.** Iceberg total freshwater flux (year 10–14 averages): ORCA025 SH (upper left); ORCA2 SH (upper right); ORCA025 NH (lower left); ORCA025 SH (lower right).





GMDD
7, 5661–5698, 2014
NEMO-ICB (v1.0)
R. Marsh et al.



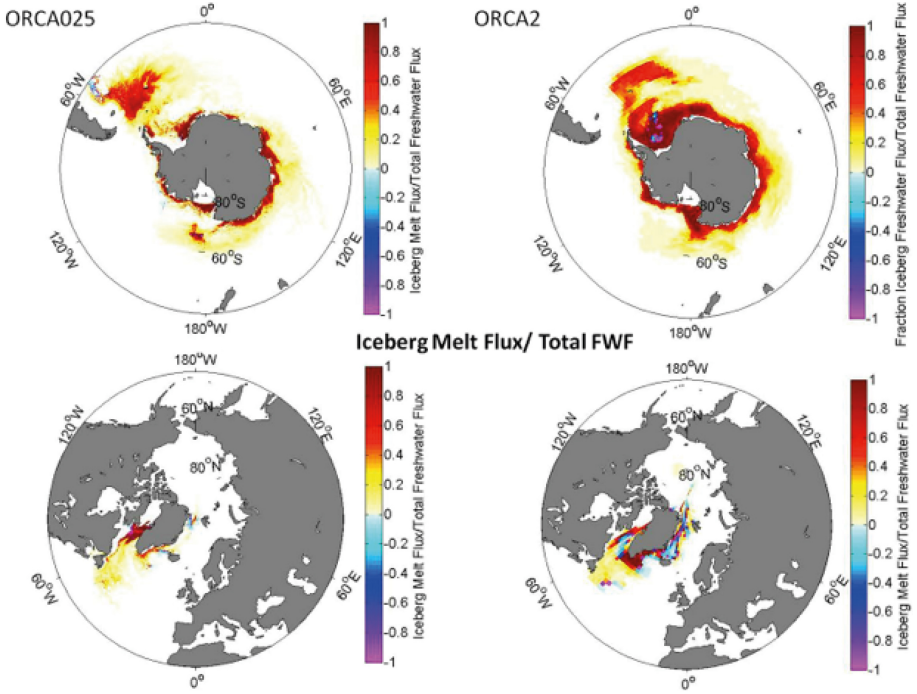


**Figure 4.** Fractions ($-1 < 0 < 1$) of iceberg freshwater flux to net freshwater flux: ORCA025 SH (upper left); ORCA2 SH (upper right); ORCA025 NH (lower left); ORCA2 NH (lower right).





GMDD
7, 5661–5698, 2014



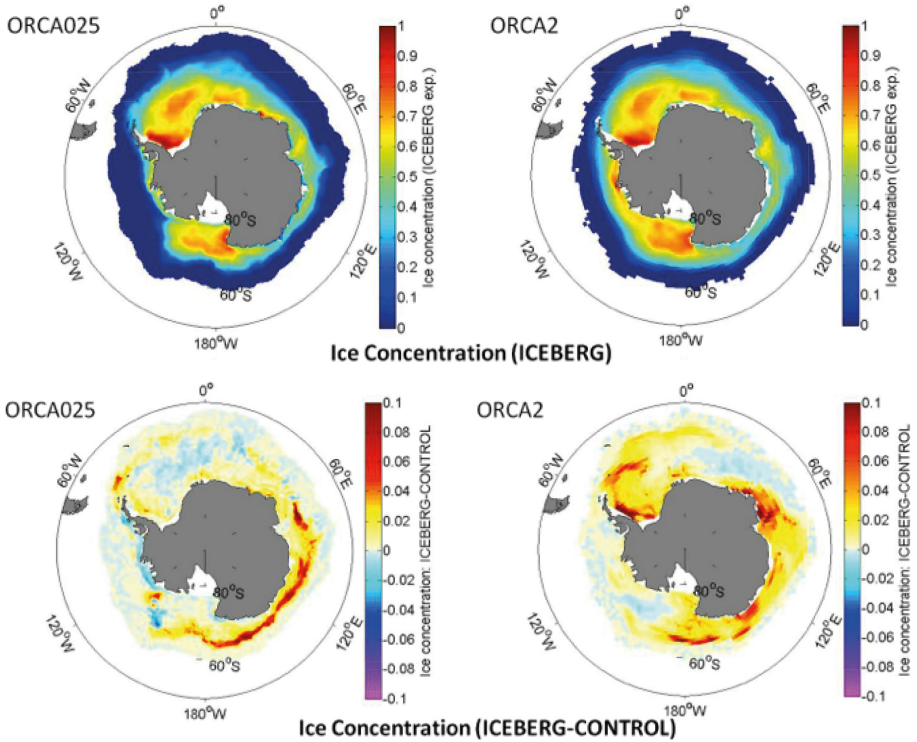


**Figure 5.** Sea ice concentration (year 10–14 averages) in ICEBERG, ORCA025 (upper left) and ORCA2 (upper right); ICEBERG minus CONTROL differences in ORCA025 (lower left) and ORCA2 (lower right).





GMDD
7, 5661–5698, 2014
NEMO-ICB (v1.0)
R. Marsh et al.



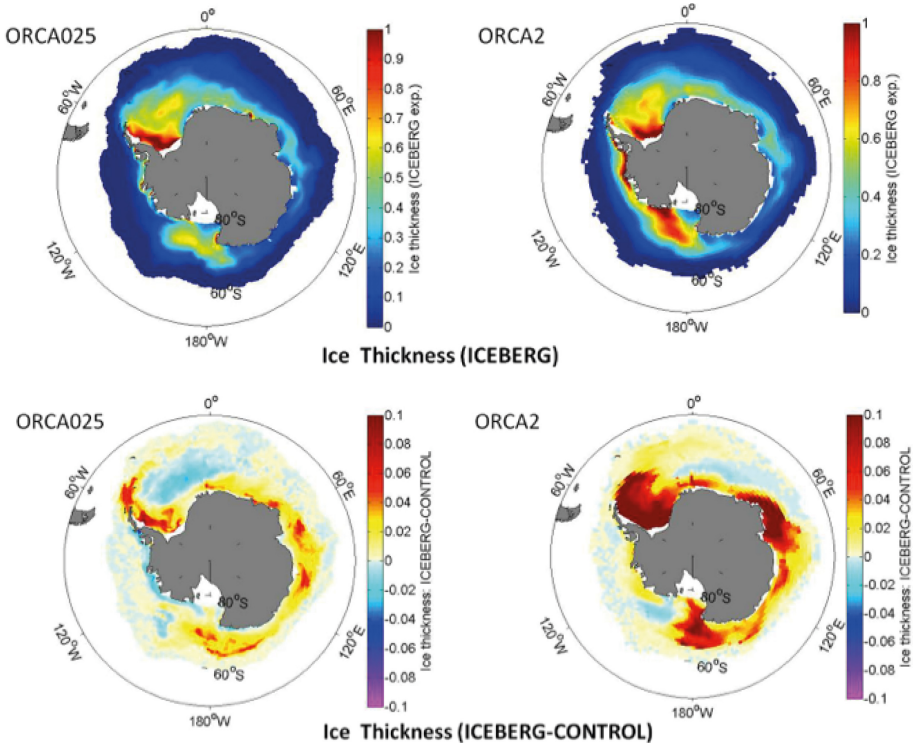


**Figure 6.** Sea ice thickness in ICEBERG, ORCA025 (upper left) and ORCA2 (upper right); ICEBERG minus CONTROL differences in ORCA025 (lower left) and ORCA2 (lower right).





GMDD
7, 5661–5698, 2014



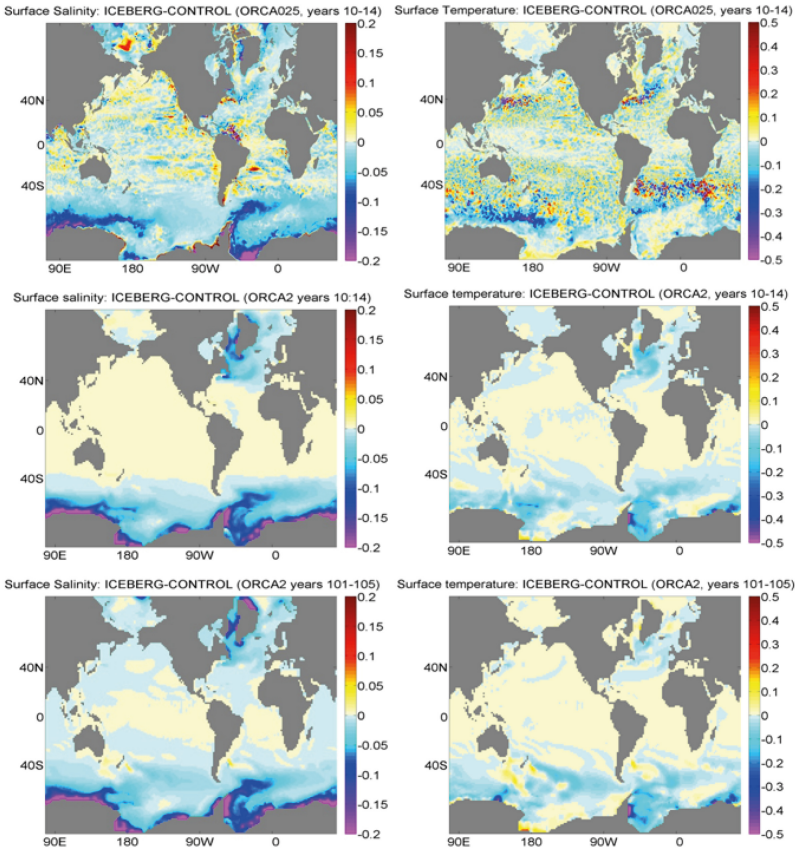


**Figure 7.** Changes at the surface: upper left – ORCA025 salinity (year 10–14 averages); middle left – ORCA2 salinity (year 10–14); lower left – ORCA2 salinity (year 101–105); upper right – ORCA025 temperature (year 10–14); middle right – ORCA2 temperature (year 10–14); lower right – ORCA2 temperature (year 101–105).





GMDD
7, 5661–5698, 2014
NEMO-ICB (v1.0)
R. Marsh et al.



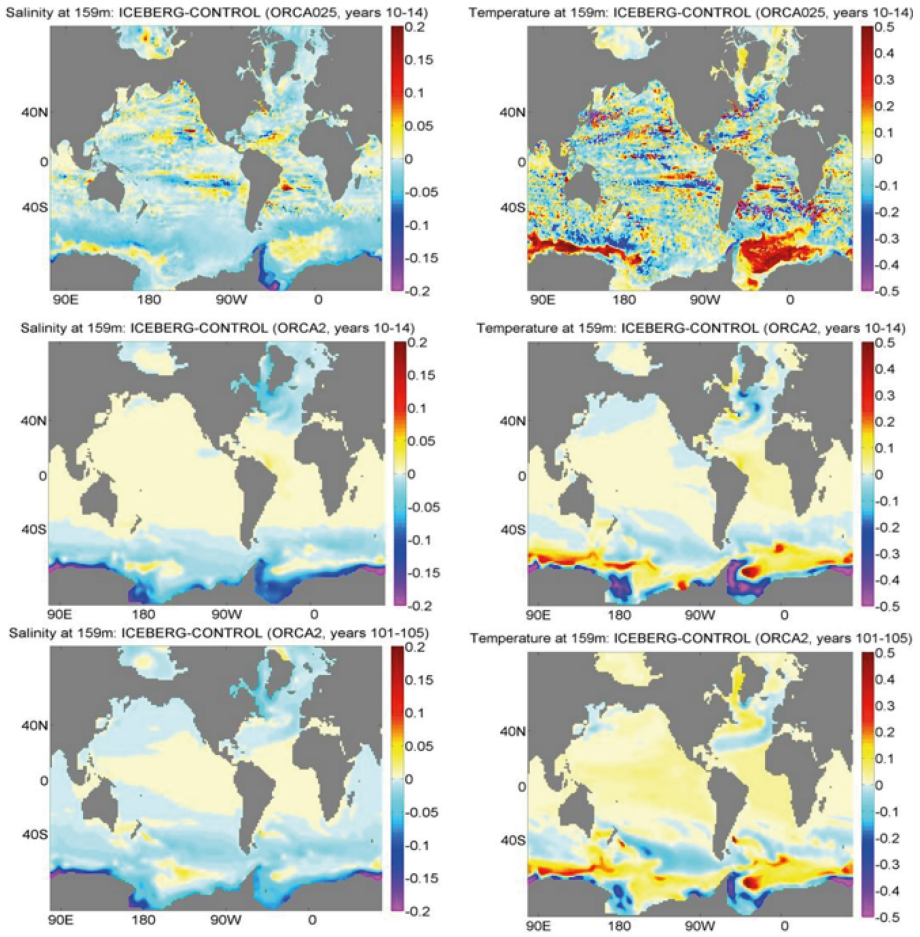


**Figure 8.** As Fig. 7, at depth level 159 m.





GMDD
7, 5661–5698, 2014
NEMO-ICB (v1.0)
R. Marsh et al.



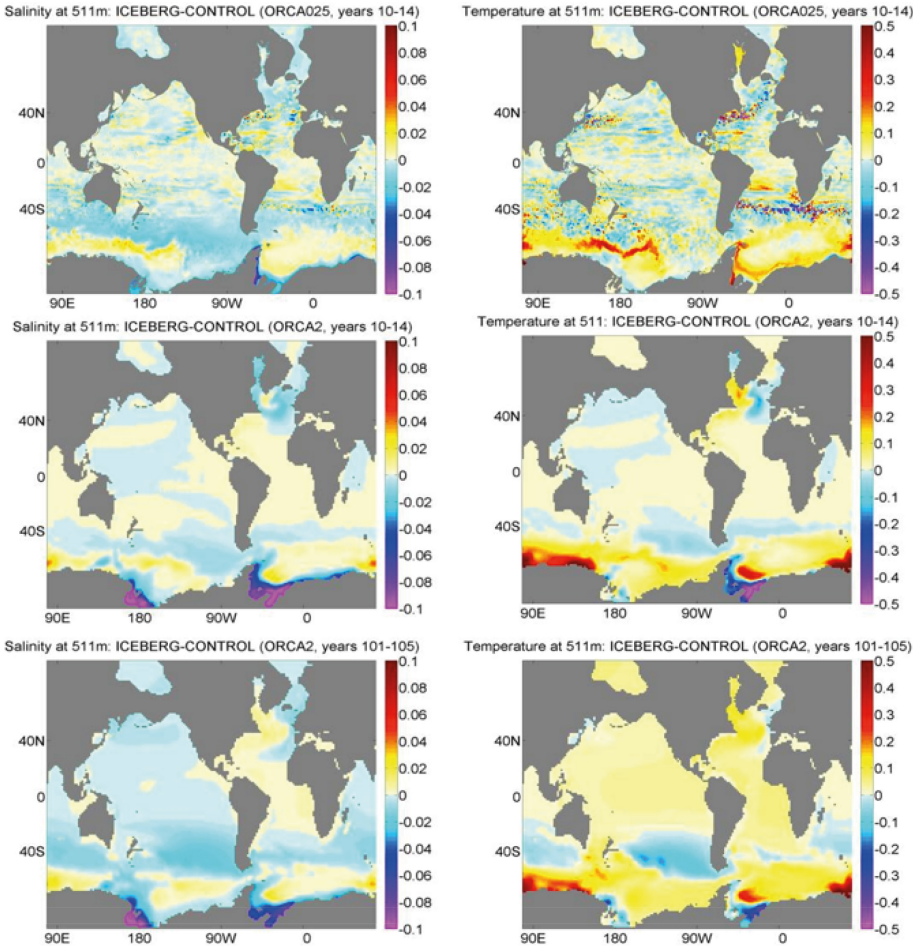


**Figure 9.** As Fig. 7, at depth level 511 m.





GMDD
7, 5661–5698, 2014
NEMO-ICB (v1.0)
R. Marsh et al.



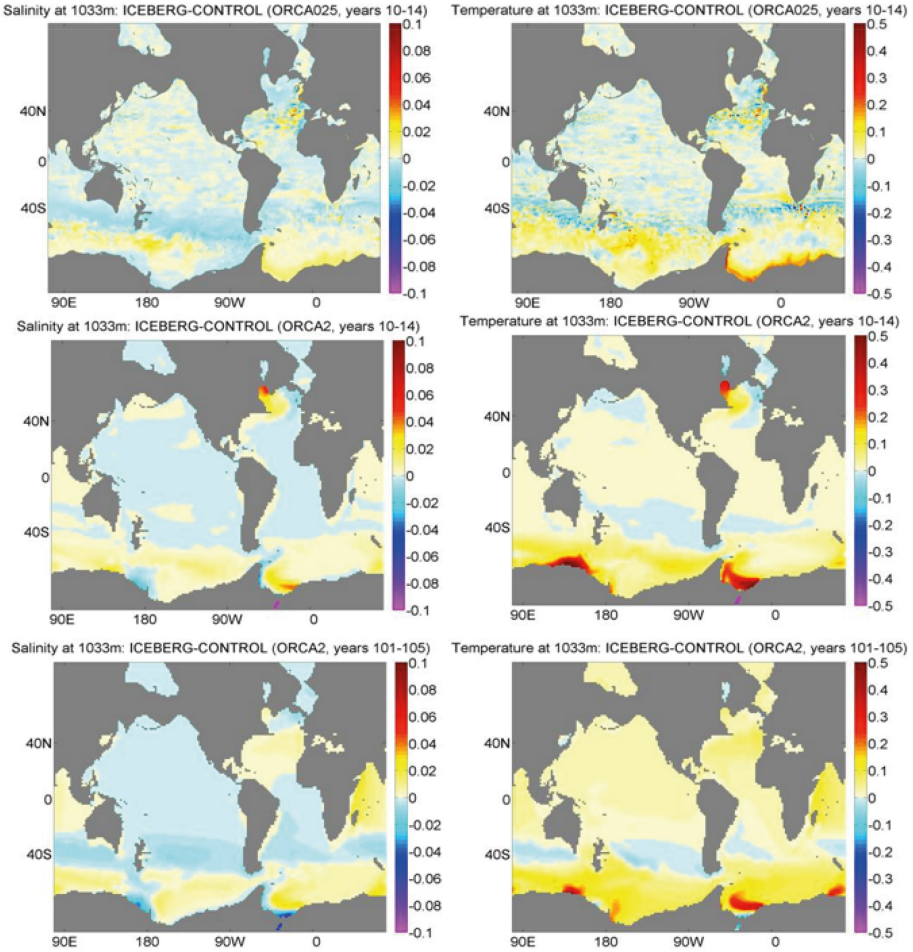


**Figure 10.** As Fig. 7, at depth level 1033 m.





GMDD
7, 5661–5698, 2014



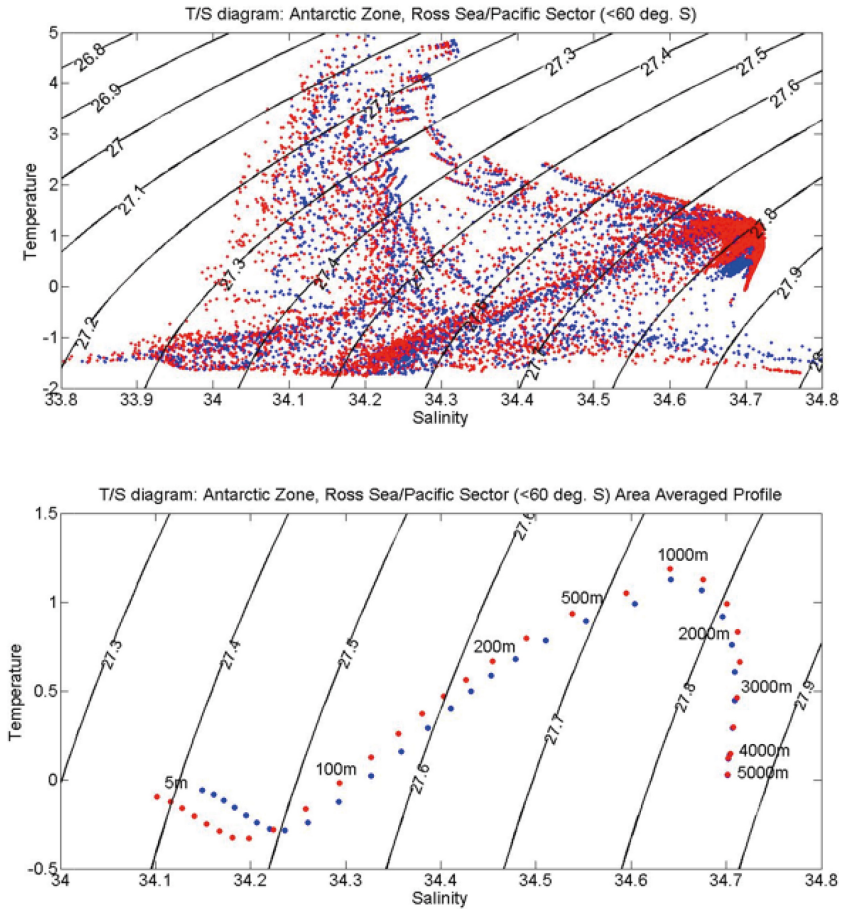


**Figure 11.** $T/S$ diagrams for Ross Sea/Pacific sector (upper panel – all data; lower panel area-averaged data), for ICEBERG (red points) and CONTROL (blue points).





GMDD
7, 5661–5698, 2014





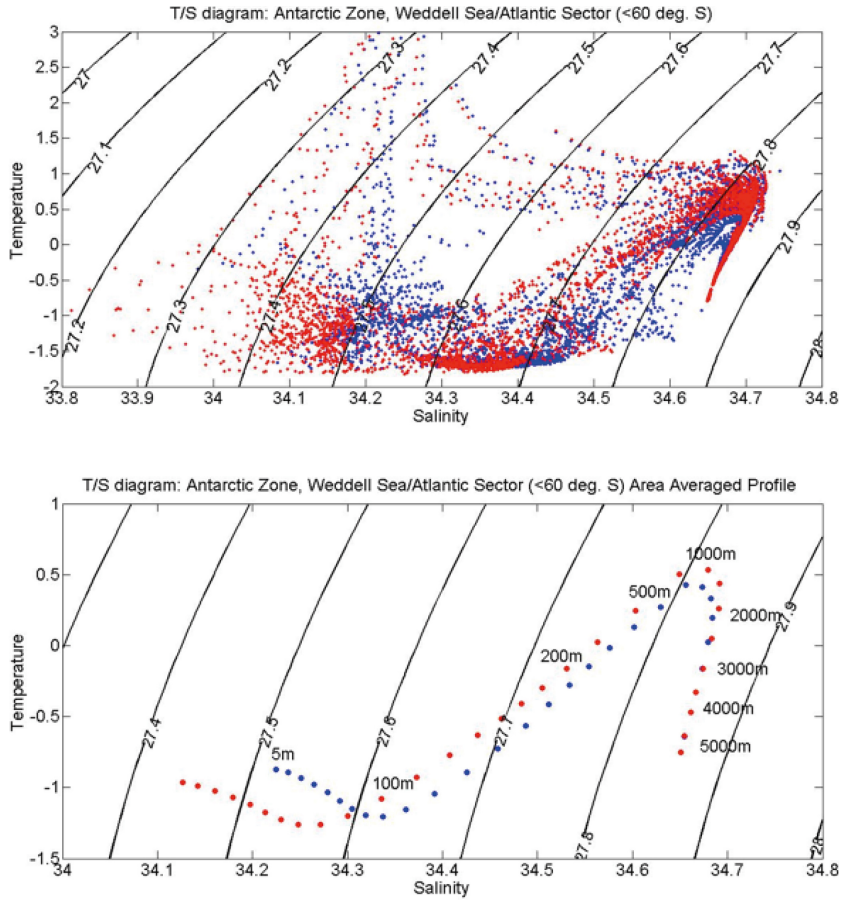


**Figure 12.** *T*/*S* diagrams for Weddell Sea/Atlantic sector (upper panel – all data; lower panel area-averaged data), for ICEBERG (red points) and CONTROL (blue points).





GMDD
7, 5661–5698, 2014



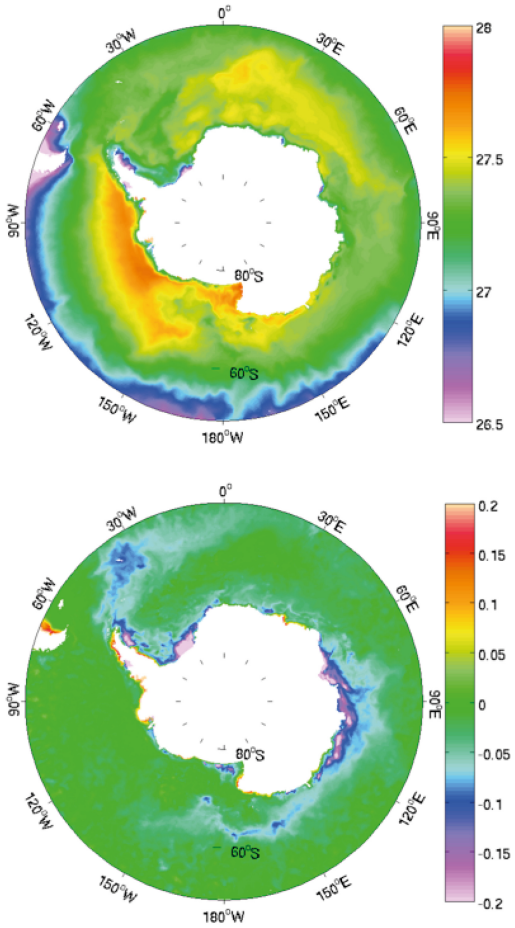


**Figure 13.** Sea surface potential density anomaly, $\sigma_0$, in ORCA025 (year 10–14 mean): ICEBERG (upper panel); ICEBERG minus CONTROL differences (lower panel).





GMDD
7, 5661–5698, 2014



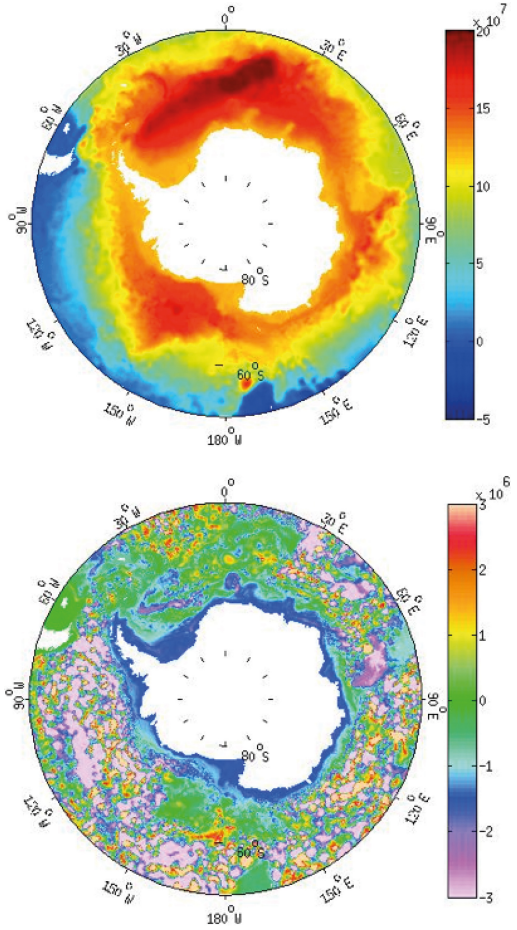


**Figure 14.** Barotropic streamfunction ($m^3\,s^{-1}$) in ORCA025 (year 10–14 means): ICEBERG (upper panel); ICEBERG minus CONTROL differences (lower panel).





GMDD
7, 5661–5698, 2014
NEMO-ICB (v1.0)
R. Marsh et al.